Platinum substituted Cobalt(II, III) Oxide: Interplay of tetrahedral Co(II) sites towards electrochemical oxygen evolution activity

Subramanian Nellaiappan[a,b 1], Navneet Jhariya[c 1], Silvia Irusta[d], Aditi Singhal[c,*]

[a]Department of Chemistry, Indian Institute of Technology Gandhinagar, Palaj, Gandhinagar 382355, Gujarat, India

[b]Department of Chemistry, Centre for Nanotechnology & Advanced Biomaterials (CeNTAB), School of Chemical and Biotechnology, SASTRA Deemed University, Thanjavur 613 401, India

[c]School of Engineering and Applied Science (SEAS), Ahmedabad University, Ahmedabad 380009, Gujarat India

[d]Department of Chemical Engineering, Nanoscience Institute of Aragon (INA), University of Zaragoza, 50018 Zaragoza, Spain

*C**orresponding Authors** E-mail address: aditi.singhal@ahduni.edu.in (A. Singhal)

1 Both authors have equal contribution

Keywords: Spinel oxide; Pt-subsituted-Co_3O_4; Solution combustion; Electrochemistry; Oxygen evolution.

Abstract

Substitution of ionic platinum is carried out in Co_3O_4 host synthesized by solution combustion strategy. These Pt substituted Co_3O_4 spinels characterized by XRD show pure crystalline phase of Co_3O_4 without any separated peaks related to Pt/PtO_x. Electrochemical OER activities of these spinels are investigated by cyclic voltammetry, linear sweep voltammetry and chronoamperometry in neutral, alkaline and neutral buffer electrolytes. LSV studies on 1% Pt substituted Co_3O_4 exhibit a low overpotential (η) of 455 mV at 20 mA cm^{-2} in KOH, as compared to PBS medium. Tafel slope value of 117 mV dec^{-1} in KOH represents one electron EC mechanism. The detailed XPS studies indicate that Pt doping increases the tetrahedral Co^{2+} sites of Co_3O_4. XPS studies before and after the OER also infers that the mixed valence of Co in the host (Co_3O_4) undergoes redox (Co^{2+}/Co^{3+}) changes with simultaneous reduction in Pt dopant from Pt^{4+} to Pt^{2+} influencing the OER activity.

1. Introduction

Spinels give potential applications in broad technical fields such as in semiconductor [1], magnetism [2-5], oxidation [6-10] and catalysis [6, 11-14]. Large class of spinels exist and researchers have worked on Magnesium spinels [2], Zinc Ferrite spinel [4], Nickel based spinels [15], Cuprospinels [16], Iron-Manganese spinels [17] and so on. Particularly, Co_3O_4 and its substituted form has been found as an effective electroactive material due to its excellent catalytic activity and corrosion reliability for electrochemical oxygen evolution reaction (OER) in alkaline media [11, 13, 18-22]. Cobalt oxide exists in two distinct forms, Co_3O_4 and CoO. Co_3O_4 spinel material exists in cubic close packing array of oxide ions that contains Co(II) ions holding the tetrahedral 8a sites and Co(III) ions in octahedral 16d sites [10, 23]. Both of these oxides show p-type semiconducting behavior but Co_3O_4 gives greater conductivity than CoO [24].

Atomic substitution is referred as one of the significant techniques to gain the desired physicochemical properties [8]. Through the defect for bearance of the spinel structure, it is feasible to substitute a notable fragment of cobalt cations by other metal ion such as *d*-and *f*-block metals [25]. It is found that iron doping improves the activity as catalyst for selective oxidation reactions [8]. Doping of zinc improves the thermal stability of spinel's core structure [26]. Platinum doping has showed positive results for oxidation and electrode modification for efficiency [9, 27]. In a latest research, computational modeling study of water splitting [6] has revealed the role of morphology based activity of cobalt oxide [28] for OER and ORR (oxygen reduction reaction) under varying pH conditions. However, controversial results still exist regarding its OER performance on size-controllable Co_3O_4 hexagonal platelets for determining active sites from two different tetrahedral and octahedral sites using density functional theory (DFT) studies and other characteristic techniques [29].

Different synthesis methods have been reported for synthesizing substituted cobalt oxides. He et al. has used the typical oriented aggregation method with binder as water for synthesizing Co_3O_4 nanocrystals [30]. Thermal decomposition method has also been adopted for copper substitution in CoO_x [31]. A facile and surfactant-free synthesis of 3.5 – 70 nm size controlled Co_3O_4 nanoparticles has been synthesized by altering the ratio of ethanol to water and utilized for the degradation of phenol [12]. Ding et al. followed a two- step procedure for the preparation of Co_3O_4 nanofibers by employing electro-spinning on aluminum foil which is followed by calcination (500^oC for 3 h) and employed as an enzyme-free sensor for glucose detection [32]. Beside these, usual methods of synthesis of spinel oxides are sol-gel [33], homogeneous precipitation [34], solvothermal synthesis [35, 36] and hydrothermal method [3, 37, 38]. Among all, solution-combustion method is used because of its unique reliability and easiness for synthesis of transition metals over spinel oxides [39].

In this paper, different percentages of platinum doping in cobalt oxide $Pt_xCo_{3-x}O_4$ (x = 0.0075 – 0.03) spinel is achieved using solution-combustion method [40, 41]. The aim of this article is (a) how this substitution affects the electrocatalytic OER activity (b) how the OER activity is correlated with the surface chemistry of Co and Pt and (c) plausible mechanism based upon the XPS investigations.

2. Materials and methods

2.1. Materials

Cobalt (II) nitrate hexahydrate ($Co(NO_3)_2.6H_2O$), 98.05 % pure, from Merck Sp. Pvt. Ltd, Mumbai, India. Hexachloroplatinic acid hexahydrate ($H_2PtCl_6.6H_2O$), 99.00 % pure, Pt content 38-40 % from Sisco Res. Lab, Mumbai, India. Urea ($CO(NH_2)_2$) 99 % pure Merck Life Sci. Pvt. Ltd. Mumbai, India. All chemicals used for this study were of analytical grade and used without

further purification. All the solutions and electrolytes were prepared using double distilled Millipore water.

2.2. Synthesis

Solution combustion method is one of the efficient and reliable methods for synthesizing the doped metal oxides and pure metal oxides [40, 42, 43]. In this work, Pt-substituted (0.25%, 0.5% and 1%) Co_3O_4 spinels were prepared. $Co_{3-x}Pt_xO_4$ (x = 0.0075 – 0.03) by dissolving 5.0 g of cobalt nitrate mixed with varying amounts of hexachloroplatinic acid (8.918, 17.9, 35.8 mg) and varied amounts of urea (0.680 – 0.687 g) in a minimal amount of distilled water in a borosilicate glass dish. For Co_3O_4 preparation, 2.0 g of cobalt nitrate is mixed with 0.688 g of urea. The clear solution containing dish is kept in a muffle furnace at 450^{o}C. After 30 minutes, the obtained powder is collected in a silica crucible and kept for calcination at 600^{o}C overnight (approximately 10 h). After calcination a black color powder is obtained and is used for various analyses. Scheme 1 represents the synthesis procedure for the Pt-substituted-Co_3O_4 and undoped pure Co_3O_4 catalysts. The synthesized materials were characterized by using the powder X-ray diffraction (XRD, BRUKER D8 DISCOVER diffractometer in the range of 20-80°), scanning electron microscopy (FESEM, Jeol, Japan), high-resolution transmission electron microscopy with electron energy disperse spectroscopy (HR-TEM: JSM - 2100, Jeol, Japan) and X-ray photoelectron spectroscopy (XPS, AXIS Ultra DLD spectroscope (Kratos) with a monochromatic Al Kα radiation (1486.6 eV, line width 0.8eV)).

2.3. Electrochemical Studies

Electrochemical studies were carried out using conventional three-electrode system using an AUTOLAB PGSTAT204 electrochemical workstation at room temperature. The electrolyte solutions were prepared by using double-distilled water. The working electrode was made using

catalyst ink which is a mixture of 100 mg of the catalyst with 100 mg of 5% Nafion solution which acts as a binder for ink. Then 650µL of isopropanol was added to make a thin ink, which was then sonicated for 20 min and then deposited on the glassy carbon (GC) electrode. The geometric area of the working electrode was 0.071cm^2. Cyclic voltammetry (CV) and linear sweep voltammetry (LSV) were carried out using catalyst coated GCE as working electrode, Ag/AgCl (sat. KCl) as reference electrode and platinum wire as counter electrode. Over potentials (η) were calculated by using the equation: $\eta = E\ (RHE) - 1.23\ V$ where $E\ (RHE) = E\ (Ag/AgCl) + (0.196 + 0.059 \times pH)$. The electrolytes used in the experiment were, 0.5 M potassium hydroxide solution (KOH; pH=13.6), 0.5 M phosphate buffer (PBS; pH=7) and 0.5 M potassium sulphate solution (K_2SO_4; pH=7). Chronoamperometry study was carried out for 1000 seconds at 1.4 V in K_2SO_4 and PBS medium and at 0.7V in KOH medium. CV (25 scans) and LSV measurements were carried out at fixed scan rates of 40 mV s^{-1} and 20 mV s^{-1} under room temperature. The double layer capacitance is of the order of 13 µF cm^{-2} for both Co_3O_4 and 1% Pt substituted Co_3O_4 confirming the comparable electroactive surface areas.

3. Results and discussions

The prepared Pt substituted Co_3O_4 ($Co_{3-x}Pt_xO_4$ (x = 0.0075 – 0.03)) and pure Co_3O_4 catalysts were characterized by XRD (Figure 1a). XRD patterns of Pt-substituted-Co_3O_4 ($Co_{3-x}Pt_xO_4$ (x = 0.0075 – 0.03)) catalysts showed sharp XRD peaks as seen in the parental Co_3O_4 spinel oxide [40, 41]. No secondary phase or peak related to Pt/PtO_x is observed however, complete substitution cannot be ascertained if some segregated phase forms on the surface. Materials appeared to be crystalline and depict large crystallite size. The morphological and microscopy analysis of 1% Pt-substituted-Co_3O_4 was characterized by SEM (Figure 1b&c) and HRTEM (Figure 1d-h). As seen in SEM images, 1% doping concentration of Pt showed well-defined

particles with hexagonal geometry with very large agglomerates of 1% Pt-substituted-Co_3O_4 (Figure 1b&c). Morphology is similar to unsubstituted Co_3O_4 [40]. Likewise, HRTEM images of 1% Pt-substituted-Co_3O_4 sample showed hexagonal morphology can be seen (Figure 1d) and the particle shape and boundaries are clearly noticeable with pure Co site and Pt-substituted- Co_3O_4 (Figure 1e). Size of the particles remain in the range of 60–120 nm and the lattice d-spacing of Pt and Co is ~0.22 and ~0.46 nm, corresponding to Pt(1 1 1) and Co(1 1 1) [44, 45]. Segregation of Pt in Pt substituted Co_3O_4 explains that complete substitution of Pt in Co_3O_4 could not be achieved. EDS studies confirms the existence of low concentration of Pt (0.3%) in the 1% Pt-substituted-Co_3O_4 sample (Figure 1h) which means that either there is heterogeneity or irregular distribution of Pt in the Co_3O_4 particles.

Similarly, high resolution XPS spectra of the Co 2p and Pt 4f elements of 1% Pt substituted Co_3O_4 catalyst showed the existence of ionic Pt^{4+} over host Co_3O_4 with Co^{2+} and Co^{3+} species (Figure 7). The detailed discussion of XPS analysis is available in later section. From the detailed characterizations of the Pt-substituted-Co_3O_4, as seen in Scheme 1, one can conclude that ionic Pt (i.e., Pt^{4+}) is possibly substituted into the Co^{2+} (tetrahedral) and Co^{3+} (octahedral) sites of host Co_3O_4. This fact can be confirmed as the substitution of Pt^{4+} enhances the Co^{2+} satellite peak at 786.0 eV to maintain the charge balance (Figure 7a, compare lower and middle spectrum)

Cyclic voltammograms (CVs) of Co_3O_4 and Pt substituted Co_3O_4 ($Co_{3-x}Pt_xO_4$) in 0.5M KOH in the potential range of 0.0 to 1.0 V is shown in Figure 2(a-d). Undoped Co_3O_4 shows OER with a current density of 100 mA cm^{-2} (Figure 2d) at 1.0 volts in the first cycle. Noticeable redox features are seen in the CV at 0.43 and 0.49 volts belonging to Co^{2+}/Co^{3+} redox reaction [40, 41]. OER occurs with an onset potential of 0.6 V. CV of 0.25% Pt-substituted Co_3O_4 also shows cobalt redox peaks at 0.5 V and 0.42 V but the current density is suppressed compared to undoped Co_3O_4

(Figure 2a). This justifies that Pt substitution is possibly on the cobalt site. Apart from this, OER starts occurring with an onset potential of 0.6 V and reaches a maximum current density of 52.7 mA cm^{-2} at 1.0 V. This current is almost half of the Co_3O_4 (Figure 2d) thus Pt substitution decreases the activity in this electrolyte. It is possible that Pt substitution is enhancing the non-reactive tetrahedral sites of Co^{2+} in Co_3O_4 to maintain the charge neutrality in the substituted compound [29]. In case of 0.5% Pt and 1% Pt substitution, the cobalt redox peaks further suppress and the observed maximum current densities at 1.0 V are 72.3 mA cm^{-2} and 85.3 mA cm^{-2} (Figure 2b,c). Clearly, the current density is lower compared to Co_3O_4 in spite of increase in the Pt concentration. This confirms that the substituted compound indeed has lesser number of active sites than Co_3O_4. Increasing trend in the current density among Pt substituted compound is probably due the Pt effect alone.

Likewise, CV of all synthesized catalysts in 0.5M K_2SO_4 at three different positive potential ranges (from 0 to 1.2 V, 1.4 V, and 1.6 V) was carried out. Since there is no OER activity in the potential range from 0 to 1.2 V, this range was increased up to 1.6V to accelerate the catalytic responses as shown in Figure 3(a–d). As seen in the CV, peak appearing between 1.2 ~ 1.6 V is belonging to Co^{2+}/Co^{3+} redox reaction, as in KOH medium. In case of Co_3O_4, OER current density is 14.6 mA cm^{-2} at 1.6 V at first cycle. CV appears featureless and no redox features are noticed in this electrolyte medium. Figure 3a shows the CV of 0.25% Pt substituted Co_3O_4. The current density at 1.6 V is 22.3 mA cm^{-2} at first cycle which is higher than Co_3O_4 alone. With 0.5% Pt and 1% Pt substituted Co_3O_4 catalysts, CV appear similar with decrement in current densities. At 1.6 V, the noticed current densities are 20.3 mA cm^{-2} and 17.4 mA cm^{-2} for 0.5 and 1% Pt substituted Co_3O_4 (Figure 3b,c). Thus, lower doping of Pt in Co_3O_4 favors OER in 0.5 M K_2SO_4 neutral

medium and activity decreases with further increases in doping concentration. This again proves that probably ionic Pt is populating the non-reactive tetrahedral site.

Although both basic and neutral electrolyte medium indicates that Pt doping is not significantly increasing the OER activity, one cannot deny the effect of local pH change near the electrode. The justification of catalytic behavior can be verified by using a neutral buffer medium for OER activity as the buffer solution will take care of the local pH effects near the electrode. Thus, the activity will truly reflect the materials property.

CV experiments in 0.5M phosphate buffer (PBS) at three different positive potential ranges (from 0.0 V to 1.2 V, 1.4 V and 1.6 V) are shown in Figure 4(a–d). Undoped Co_3O_4 (Figure 4d) gives 52.6 mA cm^{-2} at 1.6 V. For 0.25% Pt-substituted catalyst (Figure 4a) the onset potential for OER is found be around 1.1 V (1.7 V vs. RHE) giving 480 mV of over potential. Beyond this range OER activity starts, the current density at 1.2 V is 6.1 mA cm^{-2}, at 1.4 V is 28.3 mA cm^{-2} and at 1.6 V is 51.8 mA cm^{-2}. The observed current density in 0.5 M PBS at 1.6 V is similar to undoped Co_3O_4 confirming negligible effect of Pt substituent. Likewise, CV looks similar and OER current densities at 1.6 V on 0.5% Pt, 1% Pt substituted and undoped catalyst Co_3O_4 are 52.9 mA cm^{-2}, 50.4 mA cm^{-2} and 52.6 mA cm^{-2} respectively (Figure 4b-d). Clearly, no catalytic effect is noticed after Pt substitution and with increase in the Pt concentration. Thus, the local pH effects probably cause the enhancement in current in the case of KOH and K_2SO_4 and the Pt is mostly inactive.

Usually, steady state responses are more accurate to explain the materials activity compared to potentio-dynamic responses such as CV. Therefore, chronoamperometry studies of OER in 0.5M KOH, 0.5 M K_2SO_4 and 0.5M PBS electrolyte for Pt substituted (0.25%, 0.5% and 1%) and undoped Co_3O_4 catalysts are studies and shown in Figure 5. In order to attain the steady

state current response, the potential is fixed at 0.7 V for KOH (Figure 5a), 1.4 V for K_2SO_4 and PBS medium (Figure 5b, c) for 1000 seconds. Below this potential, the OER activity was insignificant and at higher potentials, noise appears in the measurement. Corresponding steady state current densities (after 1000 s) as a function of Pt doping concentration are shown in Figure 5d. Clearly, Pt doping only marginally change the current density compared to Co_3O_4 alone confirming the inactivity of Pt in Co_3O_4.

In order to further ascertain the true activity trend, LSV experiments and Tafel slope measurements of 1% Pt-substituted-Co_3O_4 have been performed in KOH, PBS and K_2SO_4 mediums (Figure 6). From the comparative LSV, the electrochemical activity of 1% Pt-substituted-Co_3O_4 for OER in KOH medium is highest as compared to K_2SO_4 and PBS medium. The observed overpotential (η) on 1% Pt-substituted-Co_3O_4in KOH at operationally relevant current density of 20 mA cm^{-2} is 455 mV (Figure 6a) which is lower than that in PBS (η=795 mV). The overpotential value is comparable to reported cobalt oxide based materials [46, 47]. The Tafel slope values obtained for 1% Pt-substituted-Co_3O_4 electrode in KOH, PBS and K_2SO_4 are 117 mV dec^{-1}, 153 mV dec^{-1}, 219 mV dec^{-1}, respectively (Figure 6b).Tafel slope value with 120 mV dec^{-1} is defined for one electron transfer EC mechanism and is probably in the present case. Likewise, the observed overpotential on pure Co_3O_4 at 20 mA cm^{-2} is 467 mV in KOH and 804 mV in PBS (Figure 6c). It is undetermined for K_2SO_4. Respective Tafel slopes on Co_3O_4 electrode in KOH, PBS and K_2SO_4 are 141 mV dec^{-1}, 158 mV dec^{-1}, and 295 mV dec^{-1} (Figure 6d). Both Co_3O_4 and 1% Pt substituted Co_3O_4 show comparable Tafel slope confirming the similarity in the OER mechanism. Further confirmation regarding the rates of OER reaction in 1% Pt substituted Co_3O_4 and Co_3O_4 is evident from the exchange current density (i_0) calculated from the Tafel plots [48, 49]. Calculated i_0 values on 1% Pt-substituted-Co_3O_4 are 0.63 mA cm^{-2}, 3.16μA cm^{-2}, 1.26 μA cm^{-2} and on pure Co_3O_4 are

0.39 mA cm^{-2}, 2.51μA cm^{-2}, 7.9 μA $cm^{-2}$for KOH, PBS and K_2SO_4 electrolytes, respectively. No specific trend is observed in the exchange current density. In KOH Pt substitution is enhancing the activity while in other solvent is decreases. If we consider PBS free from any pH change effects, Co_3O_4 is more active than 1% Pt-substituted-Co_3O_4. This verifies the fact that Pt substitution is increasing the non-reactive tetrahedral Co^{2+} sites.

4. Evolution of Pt substituted Co_3O_4 surface chemistry

In order to understand the evolution of surface chemistry of Pt substituted Co_3O_4 catalyst under OER in 0.5 M KOH condition, pre- and post-OERXPS analysis is analyzed for this study. Our aim is to study the doping effect and mechanism by XPS. XPS is done after chronoamperometry study where scan rate is not relevant. High resolution XPS spectra of the Co 2p and Pt 4f elements of 1% Pt substituted Co_3O_4, before and after the electrochemical measurements and Co 2p of pure Co_3O_4 catalysts are shown in Figure7. Co 2p doublets (Co $2p_{3/2}$ and $Co2p_{1/2}$) along with two shakeup satellites are depicted for Co_3O_4, pre and post OER analysis of Pt substituted Co_3O_4 (Figure 7a). Satellite peak at around 786.0 eV belongs to the presence of Co^{2+} in the sample [41, 50]. After Pt doping, Co $2p_{3/2}$, shows two prominent peaks at 779.1 eV and 780.6 eV with enhanced shakeup satellite around 786.1 eV. This indicates the mixed oxidation states of cobalt and change in the composition of both the states after doping or substitution [41, 50]. Noticeably, the satellite peak at about 786.1 eV become intense after Pt substitution confirming the enhancement of Co^{2+} in the system. This happens to maintain the charge balance after Pt^{4+} insertion in the lattice. Tetrahedral Co^{2+} is known to be inactive for catalytic reaction, therefore, Pt substitution did not show significant enhancement in the OER activity. XPS spectrum post-OER of Pt-substituted Co_3O_4 looks similar to Co_3O_4 with suppressed satellite at 786.0 eV.

This may indicate that Pt is possibly coming out of the Co_3O_4 matrix. Thus, Pt substituted Co_3O_4 is unstable under positive applied potential.

In case of Pt (dopant) before OER, the Pt 4f core level XPS spectra showed two doublets of Pt $4f_{7/2}$ and Pt $4f_{5/2}$ peaks at 74.4 and 77.8 eV (Figure 7b). The deconvolution of Pt $4f_{7/2}$ suggests that the dopant Pt majorly exist in +4 oxidation state [51, 52]. Evidently, the formation of more Co^{2+} after Pt^{4+} substitution is to maintain the charge neutrality because higher valent Pt is replacing lower valent Co. XPS of Pt 4f post-OER is quite noisy and fitting is a challenge. With the best of our ability we tried to deconvoluted and the deconvoluted $Pt4f_{7/2}$ spectrum shows the formation of more Pt^{2+} at 72.4 eV and 75.7 eV [51]. This appears strange as Pt is expected to remain oxidized under positive applied potential [53]. The fact that Co^{2+} in the Pt substituted sample, again converts to Co^{3+} after OER (Figure 7a) probably causing the Pt^{4+} to get reduced and hence it comes out to the surface of Co_3O_4. During OER activity, the formation of +2 oxidation state of Pt infers the adsorption of hydroxyl group ($Pt^{2+}(OH)_{ads}$) over Pt surface [51]. Considering mixed valence states of Co and Pt ions of spinel Pt substituted Co_3O_4 oxide, OER mechanism can be explained as follows:

$$Co^{3+}_{2-2y}Co^{2+}_{1+y}Pt^{4+}_{y}O_4 \; + \; 2(OH)^- \rightarrow Co^{3+}_{2-2y+\delta}Co^{2+}_{1-\delta}Pt^{4+}_{y-\delta'}Pt^{2+}_{\delta'}O_4 \; + \; O_2\uparrow \; + \; 2H^+ \; + \; 2\bar{e} \qquad \ldots(1)$$

The overall electrochemical activity of spinel Pt-substitutedCo_3O_4 oxide can be explained by considering that mixed valence Co undergoes redox changes between Co^{2+} and Co^{3+} in agreement with the XPS spectra of Co $2p_{3/2}$. Formation of Pt^{2+} from Pt^{4+} oxidation state (Figure 7b) is due to the formation of Co^{3+} from Co^{2+} causing some Pt^{4+} to get reduced. At this stage Pt^{2+} comes out of the Co_3O_4. From this, we can conclude that the interplay of octahedral sites (Co^{3+}) and tetrahedral (Co^{2+}) along with ionic Pt affects the OER activity. Schematic representation for the surface evolution of the Pt-substituted-Co_3O_4 before and after electrochemical treatment

(Scheme 1) and the substitution of ionic Pt (i.e., Pt^{4+}) into the tetrahedral (Co^{2+}) and octahedral (Co^{3+}) sites of host Co_3O_4 which assured the formation of more tetrahedral Co^{2+} sites, Pt substituted Co_3O_4 is only marginally superior to unsubstituted Co_3O_4.

5. Conclusion

Highly crystalline, platinum substituted cobalt oxide ($Co_{3-x}Pt_xO_4$ (x = 0.0075 – 0.03)) spinel oxides has been synthesized by solution combustion method. Electrochemical OER is performed using these spinel oxides in KOH, K_2SO_4, and phosphate buffer medium. CV and chronoamperometric studies have indicated that only marginal or no improvement is noticed in the Pt substituted compound compared to Co_3O_4. This is attributed to the formation of more tetrahedral Co^{2+} after Pt^{4+} substitution. XPS studies confirmed this phenomenon. LSV experiments infer that the OER overpotential of 1% Pt-substituted-Co_3O_4 and pure Co_3O_4 at the current density of 20 mA cm^{-2} in KOH medium are 455 mV and 467 mV as compared to PBS (η=795 mV for 1% Pt-substituted Co_3O_4 and η=804 mV pure Co_3O_4). Tafel slope indicates one electron transfer EC mechanism in KOH and PBS. Exchange current density (i_0) values on 1% Pt-substituted Co_3O_4 are 0.63 mA cm^{-2} (KOH), 3.16 μA cm^{-2} (PBS) and1.26 μA cm^{-2} (K_2SO_4). No set trend in the activity is observed in the Pt substituted Co_3O_4 in comparison to Co_3O_4. Activity after Pt substitution decreases in regards to the exchange current density. This demonstrates that Pt substitution increases the tetrahedral Co^{2+} sites which do not impart any activity to the substituted compound. Detailed XPS studies indicate that during OER, mixed valence of Co in the host (Co_3O_4) undergoes redox changes involving Co^{2+} and Co^{3+} influencing the Pt^{4+}reduction to Pt^{2+} species. If one can find a suitable dopant which populates the active octahedral sites of Co_3O_4, activity improvement is expected. For example, Ni substituted Co_3O_4 has been shown to improve the OER activity of parent Co_3O_4.

Acknowledgments

A.S. acknowledges Ahmedabad University and funding support from Department of Science and Technology-SERB sponsored research project (DST SERB-EMR/2016/ 005565) for funding and fellowship. Prof. Sudhanshu Sharma from IIT Gandhinagar is gratefully acknowledged for useful discussion.

Author contributions

A.S. envisaged the idea and S.N. executed the experiments and wrote the manuscript. N.J. synthesized and characterized the materials. S.I. carried out XPS measurements. All the authors contributed to the data analysis and writing and gave approval for the final submission.

Notes

The authors declare no competing financial interest.

References

[1] S. Venkatraman, A. Manthiram, Synthesis and Characterization of P3-Type CoO2-δ, Chemistry of Materials, 14 (2002) 3907-3912.

[2] P. Canepa, S.-H. Bo, G. Sai Gautam, B. Key, W.D. Richards, T. Shi, Y. Tian, Y. Wang, J. Li, G. Ceder, High magnesium mobility in ternary spinel chalcogenides, Nature Communications, 8 (2017) 1759.

[3] G. Wang, X. Shen, J. Horvat, B. Wang, H. Liu, D. Wexler, J. Yao, Hydrothermal Synthesis and Optical, Magnetic, and Supercapacitance Properties of Nanoporous Cobalt Oxide Nanorods, The Journal of Physical Chemistry C, 113 (2009) 4357-4361.

[4] A. Meidanchi, O. Akhavan, Superparamagnetic zinc ferrite spinel–graphene nanostructures for fast wastewater purification, Carbon, 69 (2014) 230-238.

[5] C. Pan, Y.J. Lee, B. Ammundsen, C.P. Grey, 6Li MAS NMR Studies of the Local Structure and Electrochemical Properties of Cr-doped Lithium Manganese and Lithium Cobalt Oxide Cathode Materials for Lithium-Ion Batteries, Chemistry of Materials, 14 (2002) 2289-2299.

[6] M. Schilling, S. Luber, Computational Modeling of Cobalt-Based Water Oxidation: Current Status and Future Challenges, Frontiers in Chemistry, 6 (2018).

[7] C.K. Kim, Internally oxidized cobalt-rich amorphous alloys for potential magnetic recording media application, Materials Science and Engineering: B, 40 (1996) 72-79.

[8] N. Bahlawane, P.H.T. Ngamou, V. Vannier, T. Kottke, J. Heberle, K. Kohse-Höinghaus, Tailoring the properties and the reactivity of the spinel cobalt oxide, Physical Chemistry Chemical Physics, 11 (2009) 9224-9232.

[9] H. Liu, C. Li, D. Chen, P. Cui, F. Ye, J. Yang, Uniformly dispersed platinum-cobalt alloy nanoparticles with stable compositions on carbon substrates for methanol oxidation reaction, Scientific Reports, 7 (2017) 11421.

[10] Z.P. Xu, H.C. Zeng, Control of Surface Area and Porosity of Co3O4 via Intercalation of Oxidative or Nonoxidative Anions in Hydrotalcite-like Precursors, Chemistry of Materials, 12 (2000) 3459-3465.

[11] B. Cui, H. Lin, J.-B. Li, X. Li, J. Yang, J. Tao, Core–Ring Structured NiCo2O4 Nanoplatelets: Synthesis, Characterization, and Electrocatalytic Applications, Advanced Functional Materials, 18 (2008) 1440-1447.

[12] Y. Dong, K. He, L. Yin, A. Zhang, A facile route to controlled synthesis of Co3O4nanoparticles and their environmental catalytic properties, Nanotechnology, 18 (2007) 435602.

[13] F. Jiao, H. Frei, Nanostructured Cobalt Oxide Clusters in Mesoporous Silica as Efficient Oxygen-Evolving Catalysts, Angewandte Chemie International Edition, 48 (2009) 1841-1844.

[14] J. Cho, Y.J. Kim, T.-J. Kim, B. Park, Zero-Strain Intercalation Cathode for Rechargeable Li-Ion Cell, Angewandte Chemie International Edition, 40 (2001) 3367-3369.

[15] K. Shih, J.O. Leckie, Nickel aluminate spinel formation during sintering of simulated Ni-laden sludge and kaolinite, Journal of the European Ceramic Society, 27 (2007) 91-99.

[16] C.-Y. Hu, K. Shih, J.O. Leckie, Formation of copper aluminate spinel and cuprous aluminate delafossite to thermally stabilize simulated copper-laden sludge, Journal of Hazardous Materials, 181 (2010) 399-404.

[17] G.D. Rieck, F.C.M. Driessens, The structure of manganese-iron-oxygen spinels, Acta Crystallographica, 20 (1966) 521-525.

[18] X. Wu, K. Scott, CuxCo3−xO4 ($0 \leq x < 1$) nanoparticles for oxygen evolution in high performance alkaline exchange membrane water electrolysers, Journal of Materials Chemistry, 21 (2011) 12344-12351.

[19] I. Nikolov, R. Darkaoui, E. Zhecheva, R. Stoyanova, N. Dimitrov, T. Vitanov, Electrocatalytic activity of spinel related cobalties MxCo3−xO4 (M = Li, Ni, Cu) in the oxygen evolution reaction, Journal of Electroanalytical Chemistry, 429 (1997) 157-168.

[20] B. Lu, D. Cao, P. Wang, G. Wang, Y. Gao, Oxygen evolution reaction on Ni-substituted Co3O4 nanowire array electrodes, International Journal of Hydrogen Energy, 36 (2011) 72-78.

[21] B.S. Yeo, A.T. Bell, Enhanced Activity of Gold-Supported Cobalt Oxide for the Electrochemical Evolution of Oxygen, Journal of the American Chemical Society, 133 (2011) 5587-5593.

[22] Y. Li, P. Hasin, Y. Wu, NixCo3−xO4 Nanowire Arrays for Electrocatalytic Oxygen Evolution, Advanced Materials, 22 (2010) 1926-1929.

[23] A.F. Wells, Structural inorganic chemistry, Clarendon Press, Oxford, 1975.

[24] Semiconductor Nanoparticles, in: Z.L. Wang, Y. Liu, Z. Zhang (Eds.) Handbook of Nanophase and Nanostructured Materials, Springer US, Boston, MA, 2003, pp. 813-848.

[25] N.W. Grimes, The spinels: versatile materials, Physics in Technology, 6 (1975) 22-27.

[26] N. Bahlawane*, P.A. Premkumar, J. Feldmann, K. Kohse-Höinghaus, Preparation of Doped Spinel Cobalt Oxide Thin Films and Evaluation of their Thermal Stability, Chemical Vapor Deposition, 13 (2007) 118-122.

[27] B.P. Vinayan, R. Nagar, N. Rajalakshmi, S. Ramaprabhu, Novel Platinum–Cobalt Alloy Nanoparticles Dispersed on Nitrogen-Doped Graphene as a Cathode Electrocatalyst for PEMFC Applications, Advanced Functional Materials, 22 (2012) 3519-3526.

[28] P.W. Menezes, A. Indra, D. González-Flores, N.R. Sahraie, I. Zaharieva, M. Schwarze, P. Strasser, H. Dau, M. Driess, High-Performance Oxygen Redox Catalysis with Multifunctional

Cobalt Oxide Nanochains: Morphology-Dependent Activity, ACS Catalysis, 5 (2015) 2017-2027.

[29] Y. Xu, F. Zhang, T. Sheng, T. Ye, D. Yi, Y. Yang, S. Liu, X. Wang, J. Yao, Clarifying the controversial catalytic active sites of Co_3O_4 for the oxygen evolution reaction, J. Mater. Chem. A, 7 (2019) 23191-23198.

[30] T. He, D. Chen, X. Jiao, Controlled Synthesis of Co3O4 Nanoparticles through Oriented Aggregation, Chemistry of Materials, 16 (2004) 737-743.

[31] A. La Rosa-Toro, R. Berenguer, C. Quijada, F. Montilla, E. Morallón, J.L. Vázquez, Preparation and Characterization of Copper-Doped Cobalt Oxide Electrodes, The Journal of Physical Chemistry B, 110 (2006) 24021-24029.

[32] Y. Ding, Y. Wang, L. Su, M. Bellagamba, H. Zhang, Y. Lei, Electrospun Co3O4 nanofibers for sensitive and selective glucose detection, Biosensors and Bioelectronics, 26 (2010) 542-548.

[33] F. Švegl, B. Orel, I. Grabec-Švegl, V. Kaučič, Characterization of spinel Co3O4 and Li-doped Co3O4 thin film electrocatalysts prepared by the sol–gel route, Electrochimica Acta, 45 (2000) 4359-4371.

[34] R. Xu, H.C. Zeng, Dimensional Control of Cobalt-hydroxide-carbonate Nanorods and Their Thermal Conversion to One-Dimensional Arrays of Co3O4 Nanoparticles, The Journal of Physical Chemistry B, 107 (2003) 12643-12649.

[35] X. Wang, X. Chen, L. Gao, H. Zheng, Z. Zhang, Y. Qian, One-Dimensional Arrays of Co3O4 Nanoparticles: Synthesis, Characterization, and Optical and Electrochemical Properties, The Journal of Physical Chemistry B, 108 (2004) 16401-16404.

[36] J.W. Schultze, Sergio Trasatti (Ed.): Electrodes of Conductive Metallic Oxides, Part A. Elsevier Scientific Publishing Company, Amsterdam, New York 1980. Preis: 83.00 US $, 170.00 Dfl, Berichte der Bunsengesellschaft für physikalische Chemie, 85 (1981) 461-462.

[37] M.M. Rahman, A. Jamal, S.B. Khan, M. Faisal, Fabrication of Highly Sensitive Ethanol Chemical Sensor Based on Sm-Doped Co3O4 Nanokernels by a Hydrothermal Method, The Journal of Physical Chemistry C, 115 (2011) 9503-9510.

[38] Y. Yao, Z. Yang, H. Sun, S. Wang, Hydrothermal Synthesis of Co3O4–Graphene for Heterogeneous Activation of Peroxymonosulfate for Decomposition of Phenol, Industrial & Engineering Chemistry Research, 51 (2012) 14958-14965.

[39] A. Varma, A.S. Mukasyan, A.S. Rogachev, K.V. Manukyan, Solution Combustion Synthesis of Nanoscale Materials, Chemical Reviews, 116 (2016) 14493-14586.

[40] A. Singhal, A. Bisht, A. Kumar, S. Sharma, One pot, rapid synthesis of Co_3O_4 by solution combustion method and its electrochemical properties in different electrolytes, Journal of Electroanalytical Chemistry, 776 (2016) 152-161.

[41] A. Singhal, A. Bisht, S. Irusta, Enhanced oxygen evolution activity of $Co_{3-x}Ni_xO_4$ compared to Co_3O_4 by low Ni doping, Journal of Electroanalytical Chemistry 823 (2018) 482–491.

[42] M.S. Hegde, G. Madras, K.C. Patil, Noble Metal Ionic Catalysts, Accounts of Chemical Research, 42 (2009) 704-712.

[43] A. Varma, A.S. Mukasyan, A.S. Rogachev, K.V. Manukyan, Solution Combustion Synthesis of Nanoscale Materials, Chemical Reviews,, 116 (2016) 14493-14586.

[44] Y. Zhao, S. Chen, B. Sun, D. Su, X. Huang, H. Liu, Y. Yan, K. Sun, G. Wang, Graphene-Co3O4 nanocomposite as electrocatalyst with high performance for oxygen evolution reaction, Scientific Reports, 5 (2015) 7629.

[45] P. Wu, H. Lv, T. Peng, D. He, S. Mu, Nano conductive ceramic wedged graphene composites as highly efficient metal supports for oxygen reduction, Scientific Reports, 4 (2014) 3968.

[46] Y. Wang, T. Zhou, K. Jiang, P. Da, Z. Peng, J. Tang, B. Kong, W.B. Cai, Z. Yang, G. Zhen, Reduced Mesoporous Co_3O_4 Nanowires as Efficient Water Oxidation Electrocatalysts and Supercapacitor Electrodes Advance Energy Materials, 4 (2014) 1400696-1400701.

[47] S. Mao, Z. Wen, T. Huang, Y. Hou, J. Chen, High-performance bi-functional electrocatalysts of 3D crumpled graphene–cobalt oxide nanohybrids for oxygen reduction and evolution reactions, Energy and Environmental Science, 7 (2014) 609-616.

[48] Y.-C. Liu, J.A. Koza, J.A. Switzer, Conversion of electrodeposited $Co(OH)_2$ to CoOOH and Co_3O_4, and comparison of their catalytic activity for the oxygen evolution reaction, Electrochimica Acta 140 (2014) 359-365.

[49] A.J. Bard, L.R. Faulkner, Electrochemical Methods: Fundamental and Applications, JohnWiley & Sons, New York1980.

[50] X. Ma, W. Zhang, Y. Deng, C. Zhong, W. Hu, X. Han, Phase and composition controlled synthesis of cobalt sulfide hollow nanospheres for electrocatalytic water splitting, Nanoscale 10 (2018) 4816–4824.

[51] M. Favaro, C. Valero-Vidal, J. Eichhorn, F.M. Toma, P.N. Ross, J. Yano, Z. Liu, E. J. Crumlin, Elucidating the alkaline oxygen evolution reaction mechanism on platinum, Journal of Material Chemistry A, 5 (2017) 11634–11643.

[52] A. Bisht, P. Zhang, C. Shivakumara, S. Sharma, Pt-doped and Pt-supported $La_{1-x}Sr_xCoO_3$: Comparative activity of Pt^{4+} and Pt^0 toward the CO poisoning effect in formic acid and methanol electro-oxidation, Journal of Physical Chemistry C, 119 (2015) 14126−14134.

[53] S. Sharma, M.S. Hegde, Pt metal-CeO_2 interaction: Direct observation of redox coupling between $Pt^0/Pt^{2+}/Pt^{4+}$ and Ce^{4+}/Ce^{3+} states in $Ce_{0.98}Pt_{0.02}O_{2-\delta}$ catalyst by a combined electrochemical and x-ray photoelectron spectroscopy study, The Journal of Chemical Physics, 130 (2009) 114706-114717.

Scheme 1

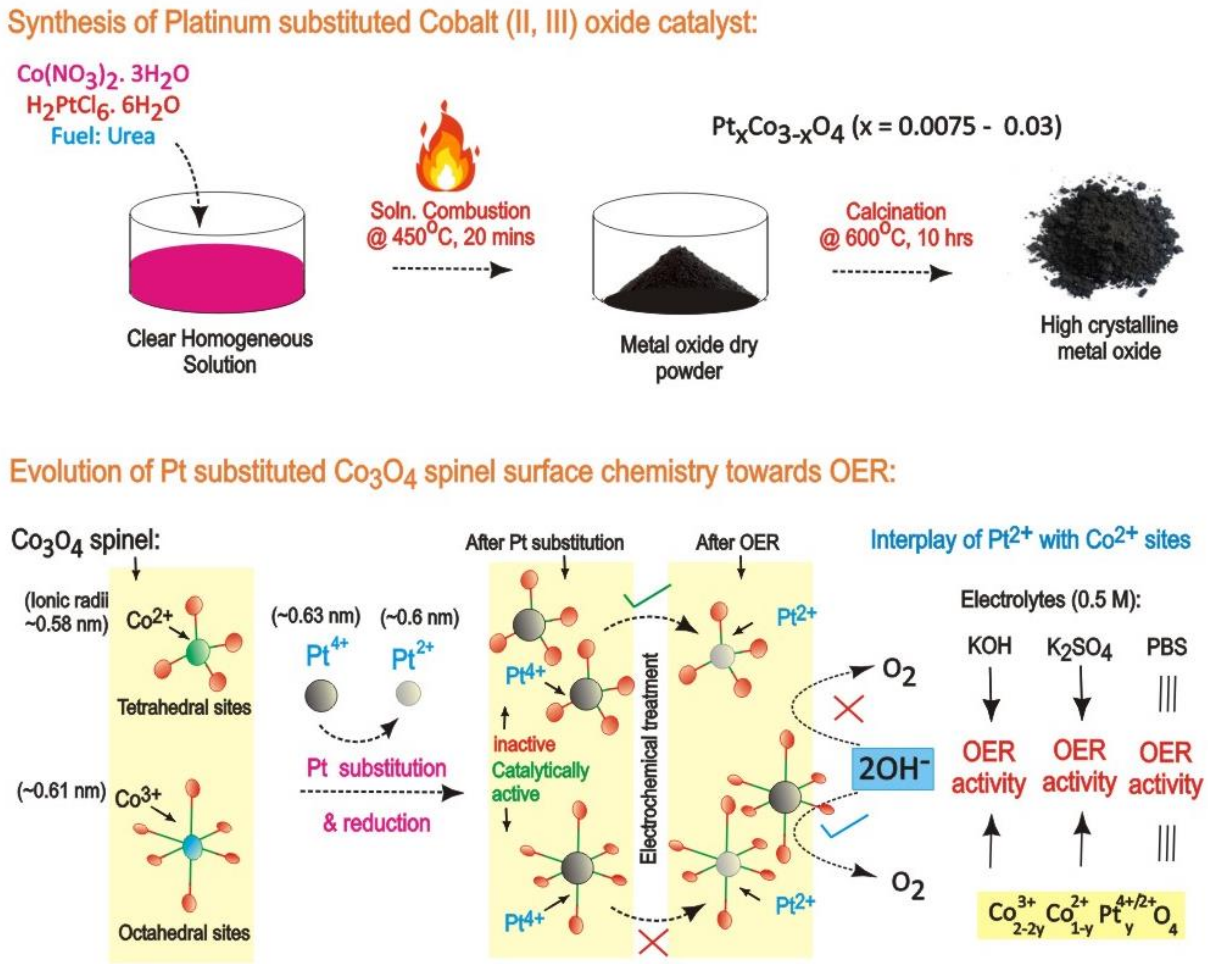

Scheme 1: Schematic representation of combustion synthesized Pt substituted Co_3O_4 and possible mechanism for the evolution of surface chemistry towards OER activity.

Figure 1

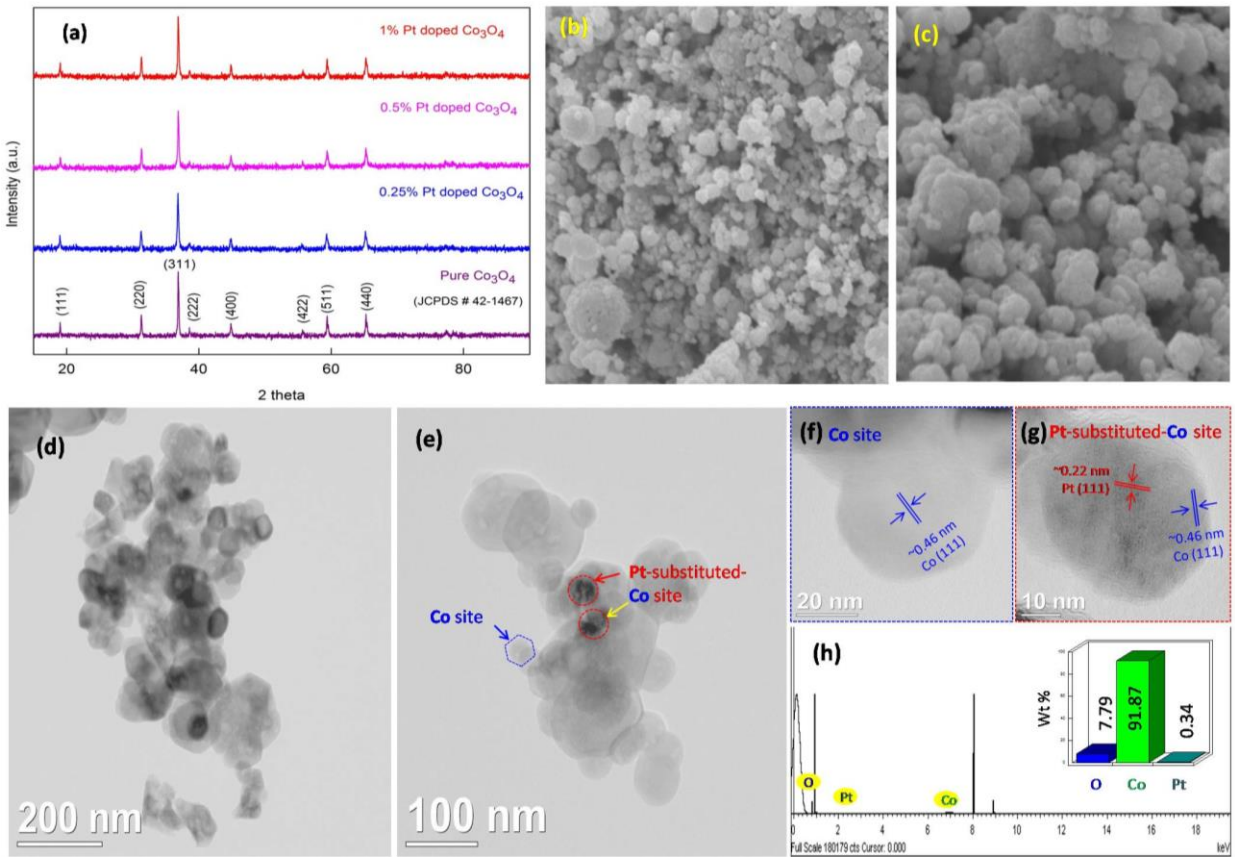

Figure 1: XRD patterns of combustion synthesized Pt substituted Co_3O_4 and pure Co_3O_4 catalysts (a). Microscope observation of the 1% Pt substituted Co_3O_4 catalyst: Low and high magnification SEM images of 1% Pt substituted Co_3O_4 (b & c), HRTEM images of 1% Pt substituted Co_3O_4 and EDS spectrum with an inset of weight percentage of Co, O, Pt atoms (d-h).

Figure 2

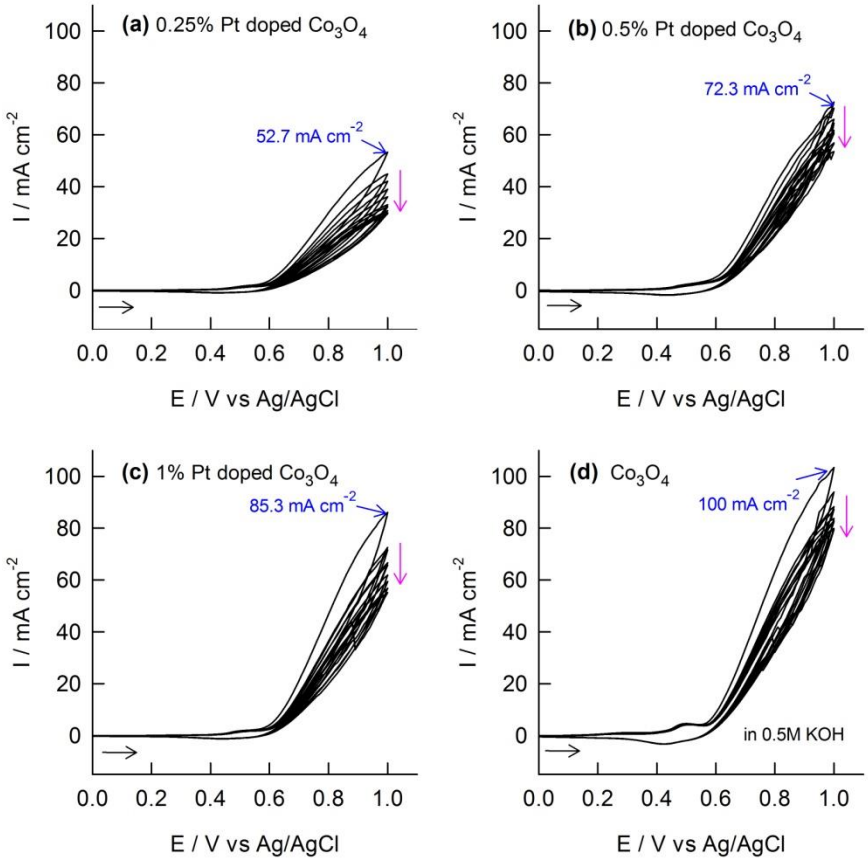

Figure 2: CV of Pt substituted Co_3O_4 catalyst for different doping percentage of Pt (a) 0.25%, (b) 0.5%, (c) 1%, and undoped Co_3O_4 (d) and at 40 mV s^{-1} of scan rate in 0.5M KOH electrolyte.

Figure 3

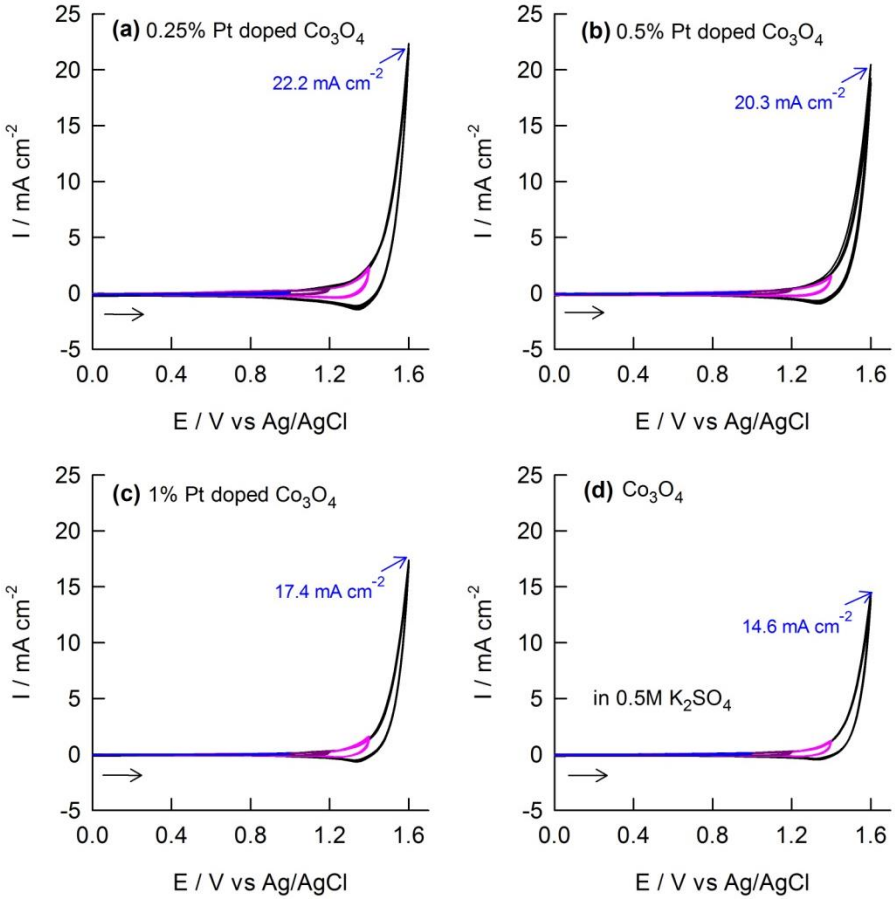

Figure 3: CV of Pt substituted Co_3O_4 catalyst for different doping percentage of Pt (a) 0.25%, (b) 0.5%, (c) 1%, and undoped Co_3O_4 (d) and at 40 mV s^{-1} of scan rate in 0.5 M K_2SO_4 neutral electrolyte.

Figure 4

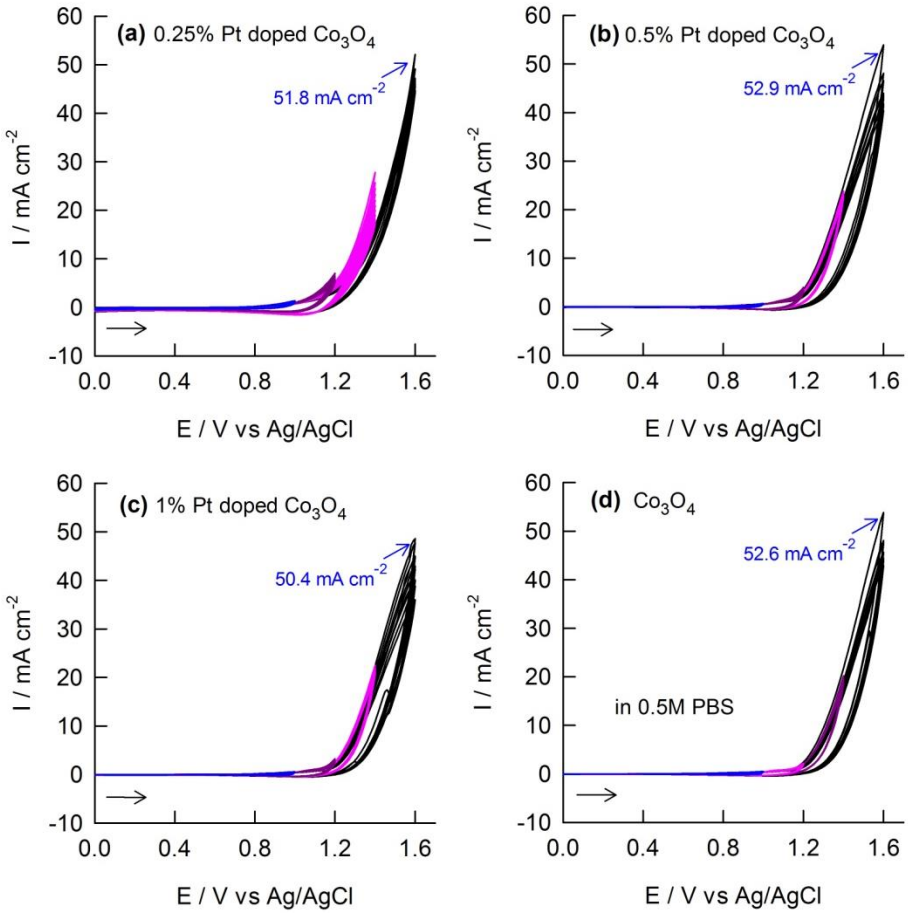

Figure 4: CV of Pt substituted Co_3O_4 catalyst for different doping percentage of Pt (a) 0.25%, (b) 0.5%, (c) 1%, and undoped Co_3O_4 (d) and at 40 mV s^{-1} of scan rate in 0.5 M PBS neutral electrolyte.

Figure 5

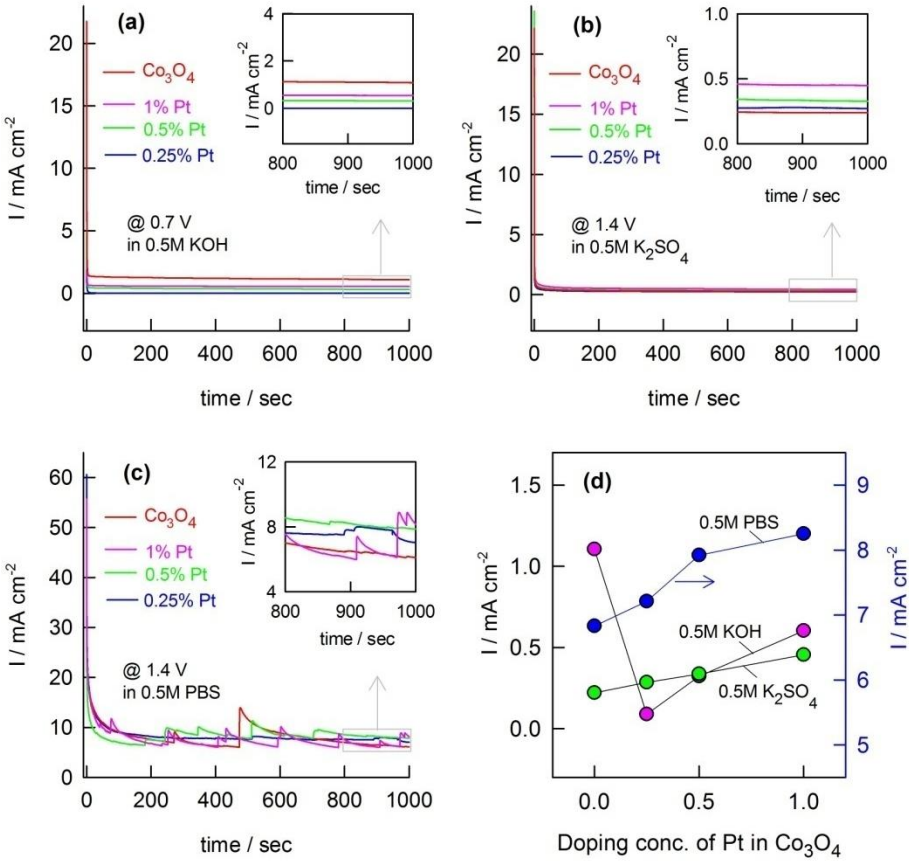

Figure 5: Chronoamperometric responses of Co_3O_4 and Pt substituted Co_3O_4 catalysts (a) at 0.7 V in 0.5M KOH and at 1.4 V in 0.5 M K_2SO_4 (b) and at 1.4 V in 0.5M PBS (c) electrolytes along with their corresponding current density after 1000 seconds with respect to Pt doping concentration (d).

Figure 6

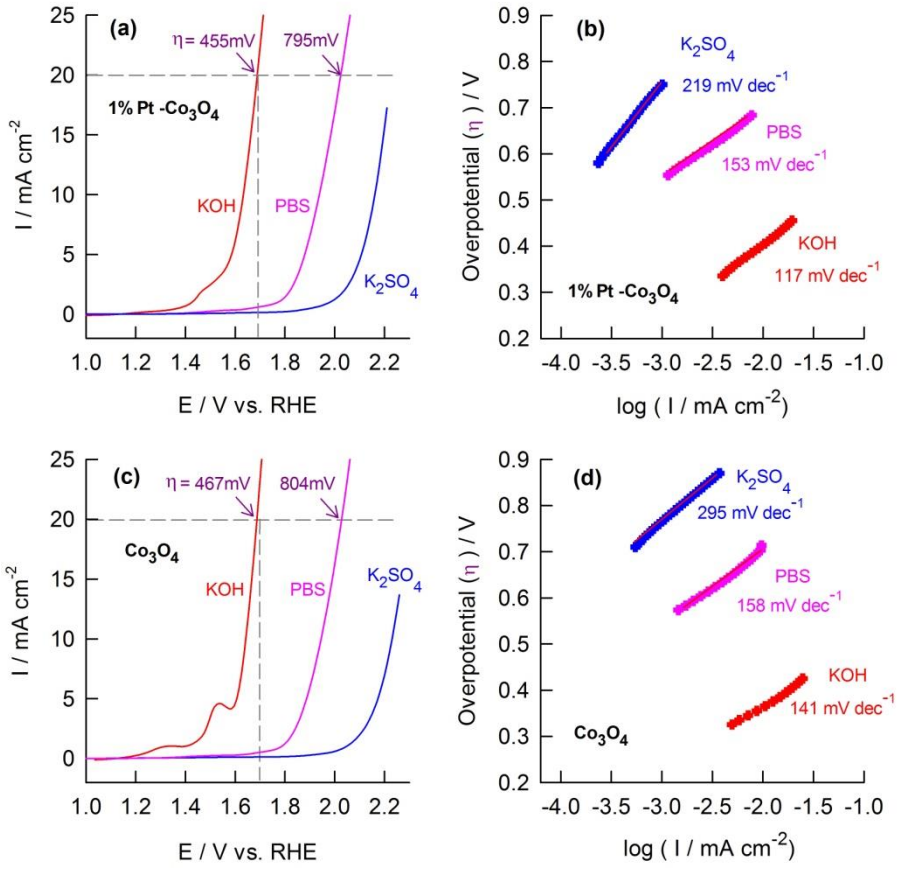

Figure 6: LSV responses of 1%Pt-substituted-Co_3O_4 (a) and undoped pure Co_3O_4 (c) at 20 mV s^{-1} of scan rate in 0.5M KOH, 0.5 M K_2SO_4 and 0.5M PBS electrolyte along with their respective Tafel plot (b and d).

Figure 7

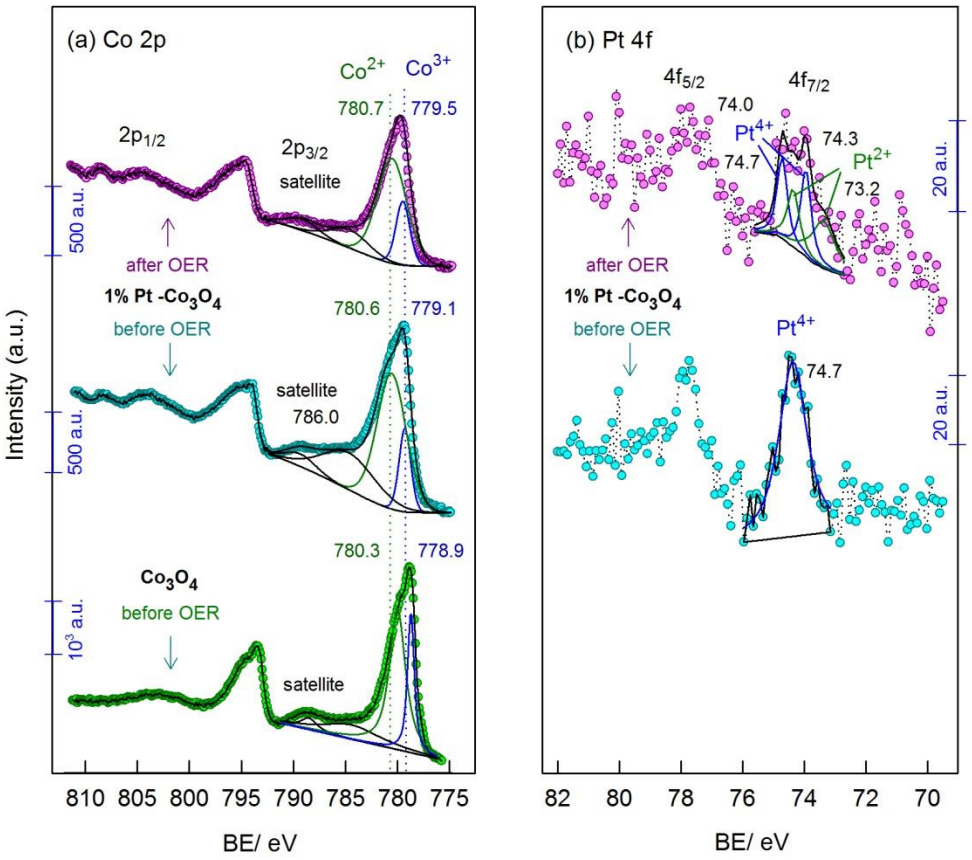

Figure 7: High resolution XPS spectra of Co 2p (a) of pure Co_3O_4 catalyst (before OER) and Pt 4f (b) region of on Pt-substituted-Co_3O_4 catalyst (before and after OER).

*****

TOC

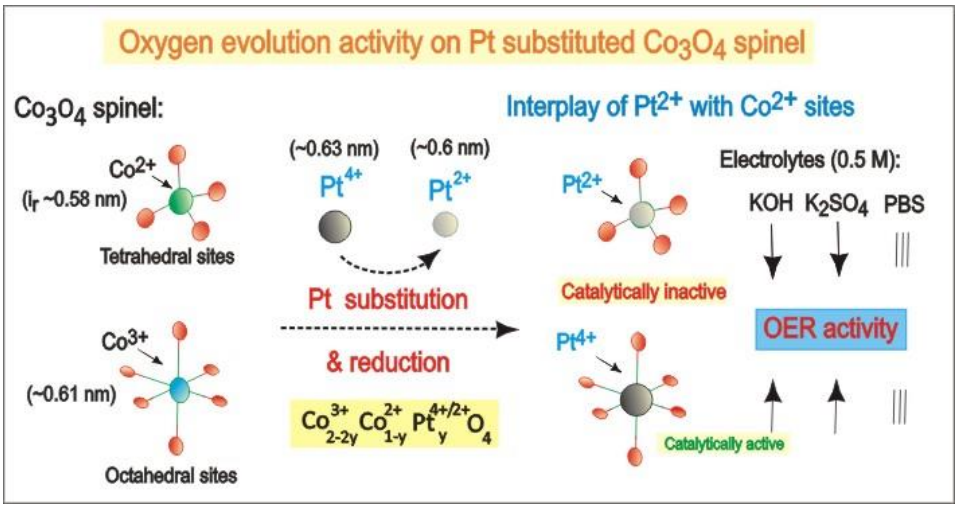
Oxygen evolution activity on Pt substituted Co_3O_4 spinel
Co_3O_4 spinel:
Co^{2+}
(i_r ~0.58 nm)
Tetrahedral sites
Co^{3+}
(~0.61 nm)
Octahedral sites
(~0.63 nm)
(~0.6 nm)
Pt^{4+}
Pt^{2+}
Pt substitution
& reduction
$Co^{3+}_{2-2y}Co^{2+}_{1-y}Pt^{4+/2+}_{y}O_4$
Interplay of Pt^{2+} with Co^{2+} sites
Pt^{2+}
Catalytically inactive
Pt^{4+}
Catalytically active
Electrolytes (0.5 M):
KOH K_2SO_4 PBS
OER activity